Computers and Concrete, *Vol.15, No.3 (2015) 411-436*
DOI: http://dx.doi.org/10.12989/cac.2015.15.3.411

Structural response of corroded RC beams: a comprehensive damage approach

Irene Barbara Nina Finozzi[a], Luisa Berto[b] and Anna Saetta*

Department of Architecture Construction and Conservation
University IUAV of Venezia, Dorsoduro 2206 - Venezia, 30123, Italy

(*Received October 13, 2014, Revised February 12, 2015, Accepted January 14, 2015*)

Abstract. In this work, a comprehensive approach to model the structural behaviour of Reinforced Concrete (RC) beams subjected to reinforcement corrosion is proposed. The coupled environmental – mechanical damage model developed by some of the authors is enhanced for considering the main effects of corrosion on concrete, on composite interaction between reinforcement bars and concrete and on steel reinforcement. This approach is adopted for reproducing a set of experimental tests on RC beams with different corrosion degrees. After the simulation of the sound beams, the main parameters involved in the relationships characterizing the effects of corrosion are calibrated and tested, referring to one degraded beam. Then, in order to validate the proposed approach and to assess its ability to predict the structural response of deteriorated elements, several corroded beams are analyzed. The numerical results show a good agreement with the experimental ones: in particular, the proposed model properly predicts the structural response in terms of both failure mode and load-deflection curves, with increasing corrosion level.

Keywords: damage model; non-linear analysis; reinforcement corrosion; cracked concrete cover

1. Introduction

The need for effective and accurate methods to predict the remaining service life of deteriorated Reinforced Concrete (RC) structures has become a priority for developing proper maintenance program and repair strategies, all over the world. In particular, all the modern Standards (i.e. National and International ones) provide for the seismic assessment of existing structures, which can be carried out only by using reliable tools for simulating and understanding the behaviour, the actual load-carrying capacity and ductility of such structures, taking into account their degradation state. One of the most severe causes of deterioration of RC structures is certainly corrosion of steel reinforcement, which may affect both ultimate strength and ductility of the structures themselves, so leading to a reduction of their level of safety. In normal condition, the alkalinity of the concrete allows the reinforcing bars to be protected by a passive film, which prevents the beginning of corrosion, but interaction with the carbon dioxide in atmosphere (i.e. carbonation process) or

*Corresponding author, Prof. Ing. Anna Saetta, saetta@iuav.it
[a]Ph.D. Student
[b]Ph.D.

http://www.techno-press.org/?journal=cac&subpage=8 ISSN: 1598-8198 (Print), 1598-818X (Online)

penetration of chlorides may create the conditions for the initiation and propagation of the corrosion phenomenon. Both carbonation and chloride attacks dissolve the passive film that protects the steel bars and in presence of oxygen and water, the steel becomes rust, which has a higher volume than the original one. The main consequence of corrosion attack is the reduction of the cross sectional area of the affected bars, in a homogeneous way in carbonated concrete and in a localized way in case of chlorides attack. The last phenomenon, known as pitting corrosion, is particularly dangerous because may lead to a significant decrease of steel area in a short time. Due to corrosion, also a marked reduction of the ultimate strain of steel is observed, as experimentally demonstrated. A further effect of corrosion, consequence of the volume expansion due to the development of the oxides, is the cracking of the concrete cover, which may lead to its spalling, with a consequent reduction of concrete section. At last, a loss of composite interaction between steel and concrete may take place, due to the weakening of the bar confinement produced by both the concrete cracking and the stirrup corrosion.

A number of studies have been devoted to non linear finite element analysis, carried out to study such effects on the structural response of RC members, using different concrete models and applying commercial as well as research FE software. Some of them have been dealt with the crucial problem of assessing the residual load-carrying capacity of corroded concrete beams, e.g. Hanjari *et al*. (2011), Coronelli and Gambarova (2004), Kallias and Rafiq (2010), Saether and Sand (2009), Biondini and Vergani (2012). The main uncertainties in the obtained results have been in ductility reduction of the corroded beams and in evaluation of the steel area reduction when pitting occurs. Moreover also the relevance of bond degradation on global structural response has not been deeply investigated, especially by varying the hypotheses of bond condition, i.e. perfect adherence, good and bad bond conditions.

In this work, a comprehensive approach to reproduce the structural behaviour of corroded RC beams is proposed, combining original formulations with some empirical/theoretical models derived from the literature, with the aim to take into account the principal effects of corrosion. In detail, concerning concrete, the coupled environmental – mechanical damage model developed by some of the authors (e.g. Saetta *et al*. 1998, 1999) is used together with a new relationship proposed to account for reduction of the compressive ductility of cracked concrete cover due to corrosion. Regarding the effect of corrosion on steel, as previously stated, the quantification of the actual steel area reduction due to corrosion is a crucial issue, particularly in presence of pitting attacks. For this reason, in this work some different methods proposed in literature for the estimation of the residual area (e.g. Biondini and Vergani 2012, Vidal *et al*. 2004, Rodriguez *et al*. 1994, Val and Melchers 1997) are considered and a sensitivity analysis of their effect on the global response of a corroded beam is carried out. A sensitivity analysis concerning different bond conditions is also carried out: different τ-slip laws, reproducing good or bad bond conditions, are considered and compared with the hypothesis of perfect adherence, for all the simulated corroded beams.

The resulting comprehensive formulation needs to be validated in order to demonstrate its ability to reproduce the structural response of RC elements in different degradation conditions. To this aim, two sound beams are analysed and the main parameters of the model are calibrated by simulating one corroded beam experimentally tested by Rodriguez *et al*. (1996), Rodriguez *et al*. (1997). Then, by using the calibrated parameters, the behaviour of the other corroded RC beams tested by Rodriguez *et al*. (1996), Rodriguez *et al*. (1997) is predicted.

2. Constitutive laws for materials

2.1 Coupled damage model for concrete

The concrete behaviour is modelled with an isotropic coupled environmental-mechanical damage model. This model, based on the work of Faria *et al*. (1998), is developed by some of the authors, Saetta *et al*. (1998), (1999) in order to couple the two mechanical parameters d^+ and d^- $\in [0,1]$, with an environmental damage parameter $d_{env} \in [0,1]$, as summarized by the following relationship, where d^{*+} and d^{*-} are the coupled damage parameters:

$$\sigma = (1 - d_{env})[(1 - d^+)\bar{\sigma}^+ + (1 - d^-)\bar{\sigma}^-] = (1 - d^{*+})\bar{\sigma}^+ + (1 - d^{*-})\bar{\sigma}^- \tag{1}$$

The environmental damage parameter is represented by an increasing function with time, $\dot{d}_{env} \geq 0$ and acts in the same way in tension and in compression. The effective stress tensor is split into two components, $\bar{\sigma}^+$ and $\bar{\sigma}^-$, related respectively to the tensile and the compressive behavior. In this way, the different non-linear behavior of concrete under tension and compression stresses and its deterioration is considered. According to such a formulation, two equivalent effective tensile and compressive stresses $\bar{\tau}^+$and $\bar{\tau}^-$ are introduced and associated to a damage criterion, similar to the Drucker-Prager one in the triaxial compression field with a cap-closure in the tensile field, and with a new mixed tension domain, Berto *et al*. (2014). The two internal damage variables, depending from the effective stresses, can be expressed as:

$$d^+ = 1 - \frac{r_0^+}{r^+} \cdot exp\left[A^+ \cdot \left(1 - \frac{r_0^+}{r^+}\right)\right] \tag{2}$$

$$d^- = 1 - \left(\frac{r_0^-}{r^-}\right)^{0.5} \cdot (1 - A^-) - A^- \cdot exp\left[B^- \cdot \left(1 - \left(\frac{r^-}{r_0^-}\right)^{0.5}\right)\right] \tag{3}$$

were r_0^+ and r_0^- are the current damage thresholds and they monitor the size of the expanding damage surfaces, A^+, A^-, B^- are material parameters. A detailed description of the model can be found e.g. in Saetta *et al*. (1998), (1999), Berto *et al*. (2014).

The model used in the present numerical analysis adopts a shear retention factor (s.r.f), as reported in Scotta *et al*. (2001), which allows to consider the secondary mechanisms of shear resistance in concrete structures by means of a s.r.f. parameter $ß_s$, whose evolution law is defined as:

$$\beta_s = 1 - \left|\frac{\varepsilon_{ij}}{\varepsilon_{ref}}\right| \geq 0 \quad i \neq j \tag{4}$$

where ε_{ij} denotes the shear deformation and ε_{ref} is a reference value of deformation which ranges between 0.001 and 0.0001 for sound beams, depending on the parameters influencing secondary mechanisms of shear resistance.

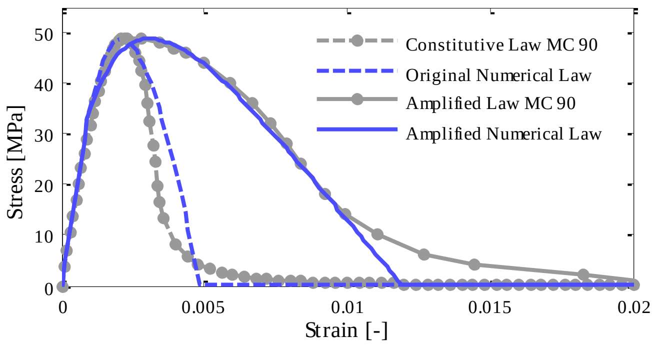

Fig. 1 Numerical and CEB-FIP MC 90 (1993) stress-strain laws for uniaxial compression of concrete

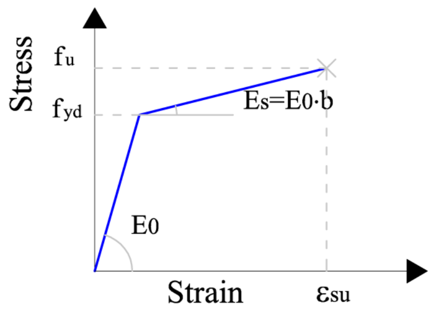

Fig. 2 tress-strain diagram for steel material

Concrete softening behaviour

As well known, the numerical analyses of strain softening materials lead to problems of strain localisation and mesh dependency. Concerning the tensile behaviour, to avoid energy problems the so called "enhanced local method", e.g. Saetta *et al*. (1999), is adopted. This simplified regularization approach considers the specific fracture energy as a function of the mesh element size *h*:

$$g_f = \frac{G_F}{h} \tag{5}$$

Regarding the constitutive law of concrete for compression, the numerical law is calibrated on the one suggested by CEB-FIP MC 90 (1993), as shown in Fig. 1 (dotted lines). As well known, e.g. CEB-FIP MC 90 (1993), Van Mier (1984) and FIB MC 2010 (2013), the compression softening branch of the uniaxial stress-strain curve is influenced by the specimen length, as well as the element geometry, the boundary conditions and the possibilities for load redistribution in the structure, and so can not be considered only as a material property. As a consequence, the constitutive relationships provided by CEB-FIP MC 90 (1993) can be reasonably accurate only for the specimen length and the characteristics of experimental test set up. Moreover, since the descending portion of the stress-strain law is size dependent, in the numerical analysis the constitutive law of concrete need to be modified as function of the mesh size to take into account the localisation of the deformations.

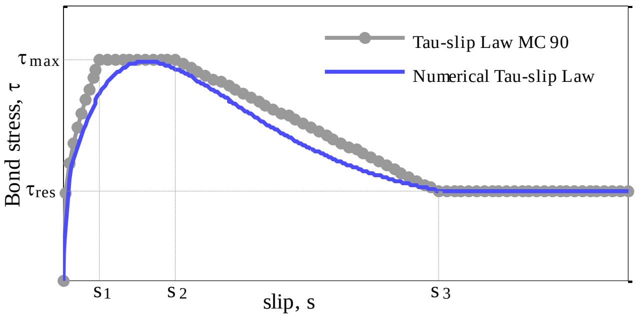

Fig. 3 Numerical and CEB-FIP MC 90 (1993) bond-stress relationship (monotonic loading)

In this work, an approach similar to the one adopted by Hanjari *et al* (2013) is used and the softening branch, first calibrated on the one of CEB-FIP MC 90 (1993) law, is amplified with the *mesh size factor*. This factor that takes into account the relation between the mesh size h and the size of the specimen (l = 200 mm) used to determine the constitutive law, Finozzi *et al*. (2014).

2.2 Steel constitutive law

The stress-strain curve of reinforcing steel is taken as for an elasto-plastic material with linear strain hardening, with a strain limit ε_{su}, as shown in Fig. 2. The model requires to define the initial Elastic Modulus E_0, the strain-hardening ratio $b = E_s/E_0$, the yield strength f_y and the ultimate strain $\varepsilon_{su.}$

2.3 Bond stress-slip law

The composite interaction between the steel bar and the surrounding concrete is commonly represented by a τ-slip relationship between the bond stress τ and the slip displacement s in the direction of the bar. In the numerical analysis, a "damage type" law τ–s developed by some of the authors is assumed, Berto *et al*. (2008). This law, after an initial linear elastic branch, shows an ascending curve up to the maximum bond stress, then a decreasing branch until a plateau corresponding to the residual bond strength $\tau_{res.}$ Such a curve is calibrated for uncorroded steel bars, considering the bond stress-slip relationships suggested by CEB-FIP MC 90 (1993), with the coefficients reported for confined concrete, Fig. 3.

3. Modeling of effects of corrosion

3.1 Effects of corrosion on concrete

Reinforcement corrosion leads to the formation of rust products, which occupy a greater volume than the original steel. For this reason concrete cover may crack and eventually spall. When corrosion attack is particularly severe and the width of the cracks exceeds a critical value, many authors have proposed to no longer consider the contribution of the concrete cover on the load carrying capacity of the structure, e.g. DuraCrete (1998), Vergani (2010). In this work, the effect of the cracking of the cover concrete is reproduced with the previously defined environmental damage parameter d_{env}, with the related reduction of concrete strength and elastic modulus till to the complete loss of mechanical properties. When d_{env} tends to the value 1, spalling of concrete cover is suitably reproduced. Moreover, the reduction of compressive ultimate strain is introduced to account for the ductility reduction due to microcraking phenomena, e.g. Coronelli and Gambarova (2004), Kallias and Rafiq (2010), Meng *et al*. (2011).

The following relationship for d_{env} is proposed:

$$d_{env} = \frac{k \ {}^{\varepsilon_1}/_{\varepsilon_{co}}}{1 + k \ {}^{\varepsilon_1}/_{\varepsilon_{co}}} \tag{6}$$

where k is a coefficient depending on bar roughness and diameter (for medium-diameter ribbed bars a value k = 0.1 has been proposed by Cape (1999) and used e.g. by Coronelli and Gambarova (2004), ε_{co} is the strain at the compressive stress peak f_c and ε_1 is the average tensile strain in the cracked concrete, which can be calculated as transverse deformation of swelling of the section:

$$\varepsilon_1 = \frac{n_{bars} \cdot w_{cr}}{b_o} = \frac{n_{bars} \cdot [2\pi \cdot (v_{rs} - 1)x]}{b_o} \tag{7}$$

where b_o is the original section width, n_{bars} the number of compressed bars, w_{cr} the average width of crack of each bar, x is the penetration of the corrosion attack, v_{rs} is the ratio of volumetric expansion of the oxides (assumed incompressible) with the respect to the virgin material, here assumed equal to 2 according to Molina *et al*. (1993). The relationships (6) and (7) are defined on the basis of concrete strength reduction, proposed by Coronelli and Gambarova, (2004).

As previously stated, as corrosion increases, the concrete becomes weaker due to microcraking occurrence and therefore a ductility decrease in compression needs to be introduced in the numerical model. In the present work, the following equation to evaluate the residual ductility of the concrete, as function of the level of corrosion affecting the reinforcement bars, is proposed:

$$\varepsilon_u^{'} = \varepsilon_u \left[1 - f\left(1 - \frac{A_{s,tot}^{'}}{A_{s,tot}}\right)\right] \tag{8}$$

where $A_{s,tot}$ and $A_{s,tot}^{'}$ are respectively the initial and the residual cross section of all the reinforcement bars, ε_u is the ultimate strain of the sound concrete and $\varepsilon_u^{'}$ is the ultimate strain of the deteriorated concrete, f is a factor that expresses the relationship between the percentage reduction of the area of the reinforcement and the reduction of the ductility of the concrete material, assumed as linear.

Finally, concerning the shear retention factor, Eq. (4), in this work the parameter ε_{ref} is assumed ranging between 0.0004 and 0.008, depending on the level of corrosion.

3.2 Effects of corrosion on steel reinforcement

When the passive film of oxide which protects the steel bar in concrete is dissolved, due to carbonation as well as chloride attack, corrosion phenomenon can start transforming steel material in rust, with the main consequence to reduce the diameter of the reinforcement bars.

In case of carbonation attack, this reduction occurs in an uniform way. The remaining cross section A'_s of each reinforcement bar, is calculated as a function of the uniform corrosion penetration x, as follows e.g. RILEM Report 14 (1996), Berto *et al*. (2008):

$$A'_s = \frac{\pi \cdot (D_0 - 2x)^2}{4} \tag{9}$$

where D_0 is the initial diameter of the reinforcement bar and the area reduction occurs around the whole perimeter of the rebar (Fig. 4a).

In presence of chloride attack, the corrosion penetration is particularly severe and localized in small regions. The so called pitting corrosion leads to a hard reduction of the cross section area and represents one of the most severe consequences of corrosion. The quantification of the residual steel area is still a controversial issue. For example Val and Melchers, (1997) have proposed a relationship which accounts for a maximum penetration of pitting p about four to eight times the average penetration (as in "uniform" corrosion) on the surface of a rebar (Gonzalez *et al*. 1995) assuming a hemispherical form of pits, and the residual area depicted in Fig. 4b. Even if with the same assumption for maximum pitting penetration, several authors (e.g. Rodriguez *et al*. (1996), Rodriguez *et al*. (1997), Saether and Sand (2009) and Khan *et al*. (2014)) have evaluated the residual area according to Fig. 4c. Fig. 5 shows the comparison of the residual reinforcing bar section at pit, for the two previously cited approaches, as the ratio p/D_0 varies. It is possible to observe an increasing difference in the evaluation of the residual area, with the increasing of the corrosion penetration.

A different approach has been used by Coronelli and Gambarova (2004) who have assumed no area reduction for pitting attack, considering a sort of balance between the strength loss due to steel area reduction and the strength increase due to hardening of the undamaged steel in the pit section.

The accelerated corrosion procedure, which is typically applied in the experimental tests, may lead to a concomitance between uniform and pitting attack at some points of the bars, i.e. a mixed corrosion type.

In this case the residual area of reinforcement can be expressed by the following formula here used to take into account both the types of corrosion:

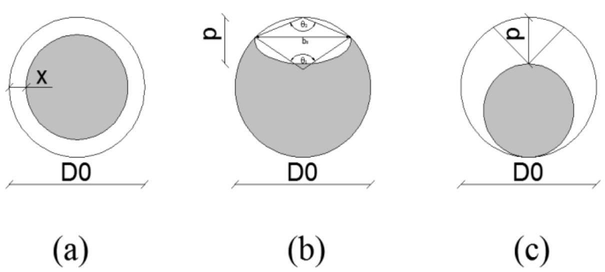

Fig. 4 Residual reinforcing bar section: a) uniform corrosion; b) pitting corrosion Val & Melchers, (1997); c) pitting corrosion Rodriguez *et al*. (1996), Rodriguez *et al*. (1997) and Khan *et al*. (2014)

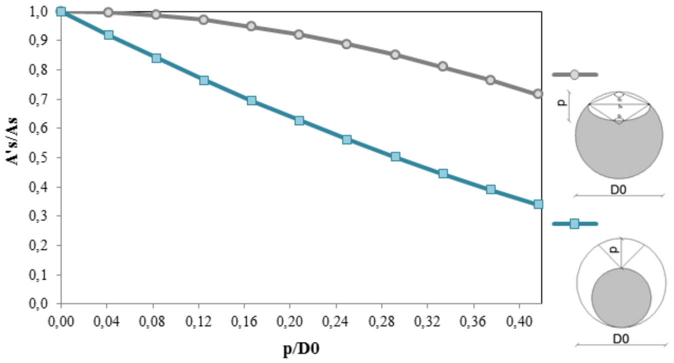

Fig. 5 Residual reinforcing bar section at pit for variable pit penetration *p*.

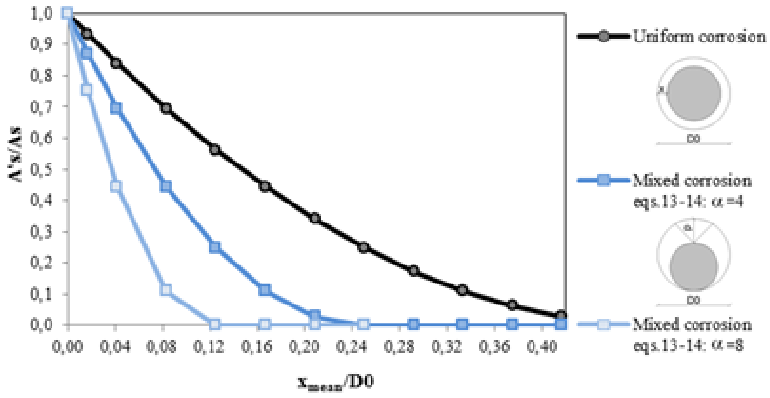

Fig. 6 Residual reinforcing bar section for variable average corrosion penetration x_{mean}

$$A'_s = \frac{\pi \cdot (D_0 - p)^2}{4} \tag{10}$$

where p is the maximum pitting attack penetration, which can be given by experimental tests or evaluated according to the following relationship, Gonzalez *et al*. (1995):

$$p = \alpha \, x_{mean} \tag{11}$$

where typical values for α, usually named pitting ratio, vary between 4 and 8 for natural corrosion, and between 5 and 13 for accelerated corrosion tests and x_{mean} is an average corrosion penetration which can be estimated from electrochemical measurements or deduced from loss in weight. The same kind of approach has been adopted e.g. by Biondini and Vergani (2012).

Therefore in this work the residual area depicted in Fig. 4c is assumed as a case of pitting corrosion with a component of uniform corrosion.

Finally, Fig. 6 shows a comparison between the residual area obtained assuming a uniform corrosion $x = x_{mean}$ and the one obtained assuming a mixed attack with the maximum depth of pit evaluated with α equal to 4 and 8.

Corrosion may affect also the mechanical properties of reinforcement steel, in particular a reduction of ultimate strain of reinforcement has been experimentally observed, especially for pitting attack. Since this effect influences the structural ductility of the RC beams, it should be considered for numerical simulation. To this aim, several relationships, depending on empirical coefficients, have been proposed in literature (e.g. Biondini and Vergani 2012, Cairns *et al*. 2005, Du *et al*. 2005a, 2005b, Castel *et al*. 2000, Kobayashi 2006, Zhu and François 2013). In this paper, the proposal of Biondini and Vergani (2012), for evaluating a plausible value of the residual ultimate strain of steel, is assumed:

$$\varepsilon'_{su} = \begin{cases} \varepsilon_{su} & 0 \le \delta_s < 0.016 \\ 0.1521\,\delta_s^{-0.4583}\,\varepsilon_{su} & 0.016 < \delta_s \le 1 \end{cases} \tag{12}$$

where ε'_{su} and ε_{su} are respectively the ultimate strain of the corroded steel and of the virgin steel, δ_s is a damage index, which provides a measure of cross-section reduction and depends on the penetration corrosion depth and on the initial diameter of the bar.

3.3 Effects of corrosion on bond

In case of corrosion, because of the development of a rust layer between bars and concrete, the reduction of the bar ribs together with the lower confinement due to cracking the concrete cover, lead to a decreasing of the adherence between concrete and steel bars depending of corrosion level. In the numerical formulation, such effect is considered introducing in the “Damage type” law τ–s, based on the CEB-FIP MC 90 (1993), a reduction of the ultimate bond strength τ_{max} and consequently of the residual bond strength τ_{res}, Fig. 3, according to:

$$d_{bond,\tau_{max}} = \frac{\tau_{max}^{degraded}}{\tau_{max}} \tag{13}$$

In addition, a reduction of the value of slip s_3, corresponding to the reaching of the residual bond stress, is considered.

In literature several experimental correlations between the level of corrosion and the degraded ultimate bond strength $\tau_{max}^{degraded}$ may be found, that depend on type of test (pull-out or bending test), material properties, geometry of the specimens, corrosion penetration *x* (e.g. Coronelli and Gambarova 2004, Rodriguez *et al*. 1994, Rodriguez *et al*. 1996, Lee *et al*. 2002, Stanish *et al*. 1999, Chung and Kim 2008, Bhargava *et al*. 2007, Cabrera 1996). Such relationships can be summarized in two different typologies:

$$\tau_{max}^{degraded} = \mathrm{A} + \mathrm{B} \cdot x^C \tag{14}$$

$$\tau_{max}^{degraded} = \mathrm{A} + \mathrm{B} \cdot e^{Cx} \tag{15}$$

It is worth noting that the values of ultimate strength, obtained with Rodriguez *et al*. (1996) expression, (14), are in general smaller than those proposed by other authors. Therefore, on the safe side, in this paper such a proposal is adopted, where the parameters A, B and C have been obtained by a linear regression analysis of the experimental data of the analysed set of beams

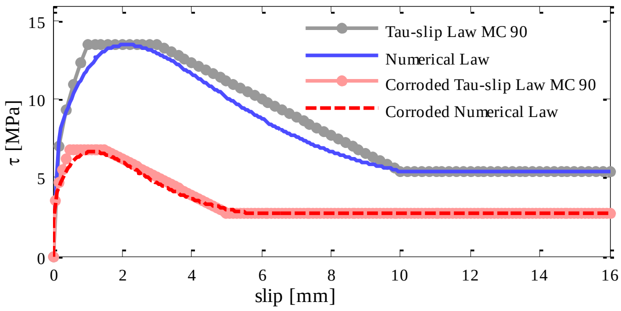

Fig. 7 Degradation of the Bond-stress law by reinforcement corrosion

(characteristic value: A = 4.75, B = 4.64, C= 1) and are valid for attack penetration between 0,05 and 1 mm and for a minimum amount of stirrups ($\rho > 0.25$). The obtained τ–s laws for sound and corroded conditions are displayed in Fig. 7.

4. Modelling of experimental test

4.1 Experimental setup and results

Rodriguez *et al*. (1996) and Rodriguez *et al*. (1997) have studied the influence of corrosion on the structural response of concrete beams by means of an extensive experimental work. In particular, six different types of beams, with different detailing, have been casted, corroded and tested to evaluate the effect of different ratio of both tensile and compressive reinforcement, concrete spalling, shear reinforcement and curtailment of bars. For a detailed description, see the reference papers Rodriguez *et al*. (1996), Rodriguez *et al*. (1997). In this work, the beams with the greater amount of steel reinforcement (type 31) are analysed, Fig. 8. Two types of beams 31 with the same geometrical characteristics have been tested:

- type 1, reference beams (sound conditions) characterized by compressive strength of 49 MPa, at the date of loading test;
- type 2, beams subjected to corrosion (degraded conditions) characterized by compressive strength of 37 MPa, at the date of loading test.

The main characteristics of the two concrete types are summarized in Table 1. Regarding the reinforcing bars, ribbed bars of Spanish type AEH 500S have been used, whose main characteristics are summarized in Table 2.

In beams type 2, calcium chloride has been added to the mixing water, then an accelerated corrosion procedure has been carried out for a period between 100 and 200 days, in order to obtain the required level of corrosion. Reinforcement bars have been subjected to a constant current density of about 100 μA/cm^2, corresponding to ten times the corrosion intensity measured in highly corroding concrete structures. Table 3 shows the duration of the accelerated corrosion for each beam and the values of the attack penetration, produced at main bars and at stirrups. The mean value of the attack penetration x_{mean} has been obtained by gravimetric method, whereas the maximum value of pitting corrosion p has been obtained by geometrical measurement on pits of each bar.

Reinforcement bars have been corroded while the beams are unloaded, then the simply supported beams have been tested up to failure under two monotonic symmetrical loads, as shown in Fig. 8. The two sound beams (311 and 312) have failed by crushing of concrete in compression, the corroded beams (313, 314, 316) have exhibited the same type of failure, but at lower ultimate loads and for lower deflections than those of the reference beams. The corroded beam 315 has instead failed by shear. In some cases, the yield stress in the tensile bars has not been reached due to the premature deterioration of top side concrete, caused by corrosion of the compression bars (314 and 316).

Table 4 summarizes the main results obtained in the experimental tests, while Fig. 9 shows the consequent load-central deflection curves for all the beams type 31 (reported load is 2P).

In order to understand the experimental results, it is necessary to remember that the compressive strength of the concrete of the corroded beams is lower than the one of the uncorroded beams. To sum up, the experimental results show that, with an increasing level of corrosion, the ultimate strength and the ultimate displacement decrease and for very high levels of attack the type of failure changes. Reduction of the reinforcement area and deterioration of the mechanical properties of the concrete covers have shown to be the most relevant effects of corrosion in the beams, with significant consequences on their structural response. Instead, the bond degradation (if it happened) in tested corroded beams 31 has not shown a significant influence on their structural behaviour mainly due to the fact that the ends of the bars are adequately anchored at support regions, Rodriguez *et al*. (1996).

Table 1 Mechanical characteristics of concrete

CONCRETE	TYPE 1	TYPE 2
f_{cm}	49 MPa	37 MPa
f_t	3.59 MPa	2.85 MPa
E_c	36518 MPa	33254 MPa
G_f	76 N/m	62 N/m

Table 2 Mechanical characteristics of reinforcing bars

Elastic Modulus		E_0=210000 MPa		
Plastic Modulus		E_s=840 MPa		
Tensed bars	ϕ12	A=113.10 mm^2	f_{sy}=585 MPa	f_{su}=655 MPa
Compressed bars	ϕ 8	A=50.27 mm^2	f_{sy}=615 MPa	f_{su}=673 MPa
Stirrups p=85 mm	ϕ 6	A=28.27 mm^2	f_{sy}=626 MPa	f_{su}=760 MPa

Table 3 Accelerated corrosion results – Beams type 31

BEAM	No. OF	ATTACK PENETRATION (mm) (+)		
No.	DAYS	TENSILE BARS	COMPRESSIVE BARS	LINKS
313	111	0.30 (1.3)	0.2	0.35 (2.8)
314	128	0.48 (1.5)	0.26	0.50 (4.0)
316	164	0.42 (1.8)	0.37	0.54 (4.3)
315	190 (*)	0.51 (2.0)	0.34	0.63 (5.0)

+ Average value x_{mean} and maximum value at pitting p (in brackets)
* Beams kept under natural corrosion conditions other 180 days

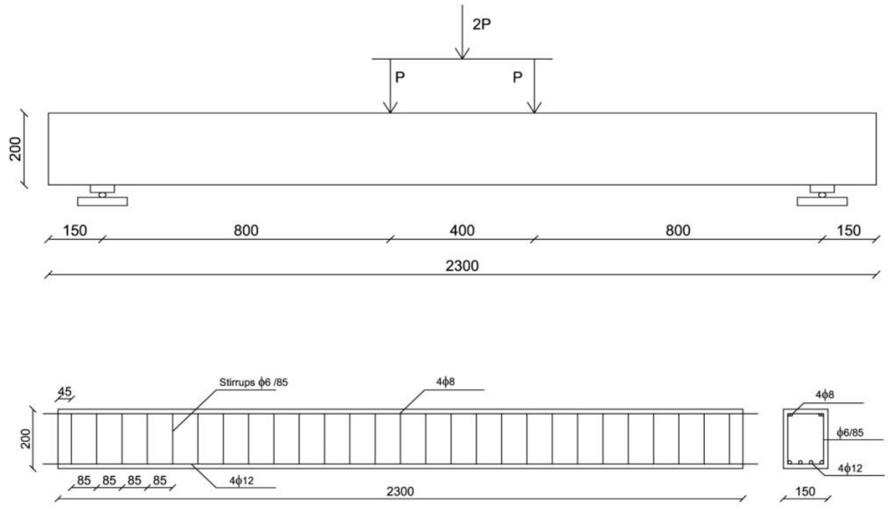

Fig. 8 Scheme of beams type 31 and loading test arrangement

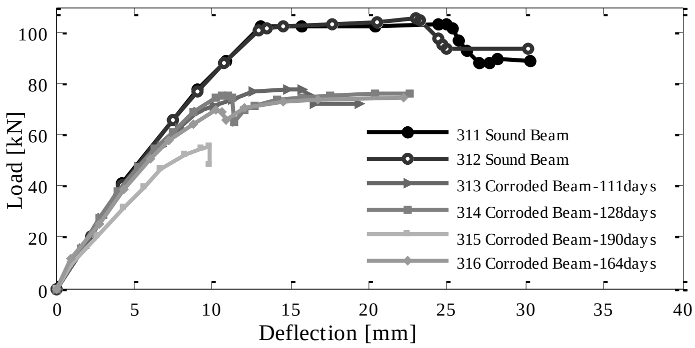

Fig. 9 Experimental results: load-deflection curves for beams type 31

Table 4 Experimental results – Beams type 31

BEAM No.	ULTIMATE LOAD		
	TYPE OF FAILURE (+)	SHEAR FORCE (kN)	BENDING MOMENT (-) (kNm)
311	2	52.3	38.1
312	2	53.2	38.8
313	2	38.7	28.2
314	2	39	28.5
316	2	37.7	27.5
315	3	27.7	20.2

(+) Type of failure: 1-bending (tensile reinforcement); 2-bending (concrete); 3-shear; 4-shear/bond
(-) maximum values obtained by equilibrium and taking account of the horizontal reaction

4.2 Numerical simulations

All the beams of type 31 tested by Rodriguez *et al*. (1996), Rodriguez *et al*. (1997) are analyzed by using the proposed comprehensive approach. Preliminary analyses are carried out on sound beams, in order to demonstrate the capacity of the damage mechanical model to well reproduce the experimental response of RC elements and to validate the proposed approach for the mesh size correction.

Concerning corroded beams, in a first phase of study the analysis of one of them is carried out in order to test and calibrate the main parameters involved in the proposed relationships characterizing the effects of corrosion (e.g. Eqs. (6) to (8), (14), (15)). Then in the second phase of study, i.e. the predictive one, analyses are performed on all the other corroded beams to predict their structural response, by using the previously calibrated values of the parameters. The obtained results are in good agreement with the experimental ones, both in terms of load carrying capacity and ductility behaviour. Hence the ability of the numerical model to capture the influence of the main effects of corrosion, at different level of degradation, on the global structural response of RC beams is demonstrated.

The coupled damage model is implemented in the finite element framework OpenSEES (Open System for Earthquake Engineering Simulation), Mckenna *et al*. (2000) and the concrete beams are modeled with a regular mesh of 15x15mm size of quadrilateral plane stress elements. Steel bars are modeled with truss elements and zero-lengths elements are placed between steel bars and concrete elements, having different bond laws, in order to simulate: perfect adherence between the two materials, slip occurrence, defined by a damage type law τ–s and reduction of the composite interaction due to corrosion, as described in Sect. 3.3.

4.2.1 Reference beams

The two reference beams (311-312) are preliminary analysed in order to validate the proposed approaches for the mesh size correction. Actually, while the correction here adopted in tension is well known and widely used, the approach adopted for the compression softening behaviour needs a validation phase. As described in Sect. 2.1 the constitutive law suggested by CEB-FIP MC 90 (1993) for concrete type 1 is amplified by the *mesh size factor*, to partially overcome the problem of mesh size dependency in compression. The adopted damage numerical law is also amplified accordingly, Fig. 1, and used to simulate the experimental test. The mechanical characteristics adopted in the numerical model for steel material and concrete are listed in Table 1 and Table 2. It is worth noting that such values are based on experimental data and on CEB-FIP MC 90 (1993) recommendations. Firstly, perfect adherence hypothesis between the concrete and steel bars is considered.

Fig. 10 shows the comparison between numerical and experimental Force-displacement curves. The main difference concerns the initial stiffness, which is significantly higher in the numerical response. This effect could be due to a precracking phase, missing in the experimental test, which seems to start directly with the cracked stiffness. Indeed, if the numerical curve is shifted of a value corrisponding to the beginning of cracking phase (dashed line, Fig. 10), the initial stiffness closely corresponds to the experimental one. It is worth noting that both the experimental failure load and ultimate displacement are well captured by the numerical simulation.

Due to the percentage of tensile and compressive reinforcement bars and stirrups, RC beams of type 31 have presented a ductile flexural mode of failure, with yielding of tensile reinforcement

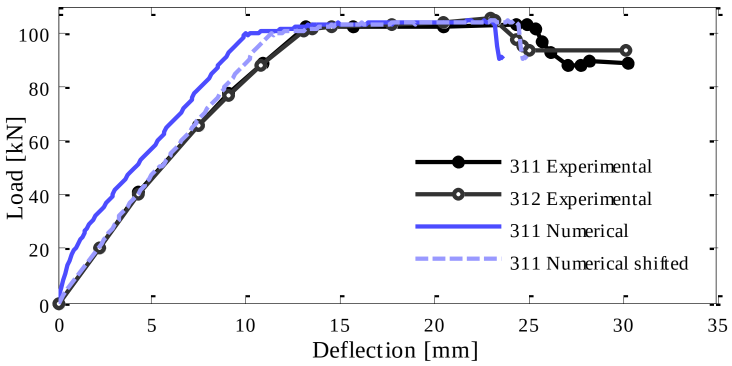

Fig. 10 Force-deflection curves for sound beams 311-312

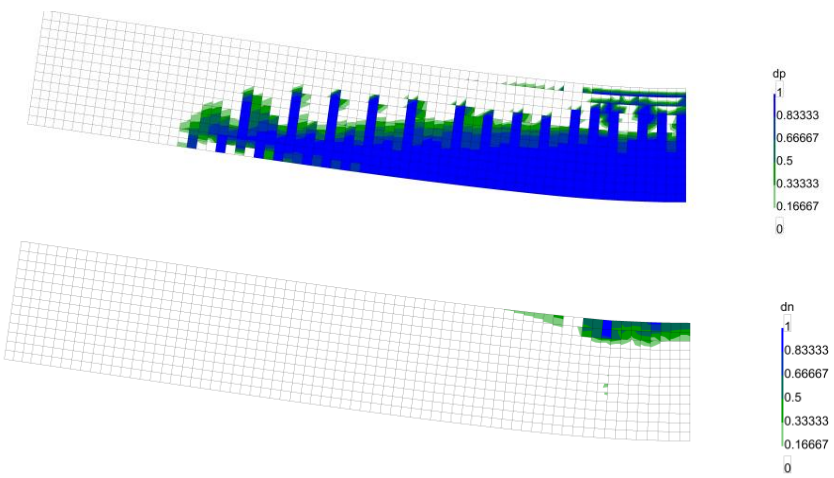

Fig. 11 Tensile (dp) and compressive (dn) damage contours for sound beams 311-312

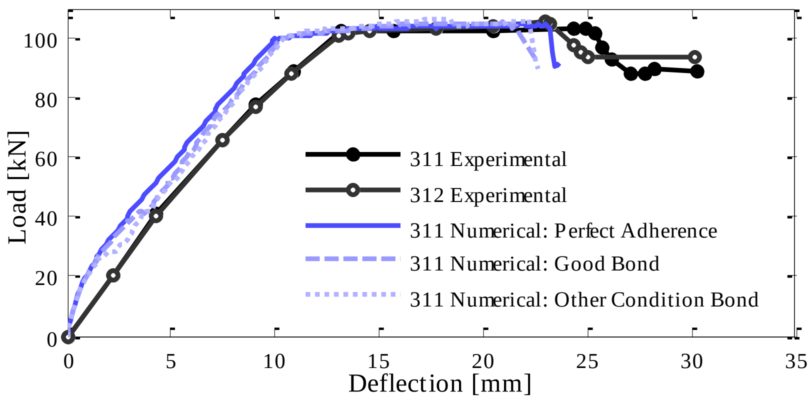

Fig. 12 Force-deflection curves for sound beams 311-312 with different bond conditions

long before crushing of concrete in the upper zone. The same type of failure is obtained in the finite element simulations: the long horizontal plateau, Fig. 10, characterized by the presence of flexural cracks, precedes the failure by crushing in the upper-central zone of the beam, as shown in Fig. 11 depicting the positive and negative damage contours.

A sensitivity analysis about different bond condition is also carried out, in order to reproduce the experimental observations, i.e. Rodriguez *et al*. (1996), Bertagnoli *et al*. (2006), of non-influence of bond on structural response of such beams. Since the beams 311-312 are not corroded, the damage type τ–s laws are calibrated to the ones of CEB-FIP MC 90 (1993) for the cases of "Good Bond" and "Other Condition". Fig. 12 shows the comparison between the assumed bond conditions and the case of perfect adherence, demonstrating that different bond stress-slip laws slightly influence both the failure load of the beam, which remains substantially unchanged, and the ductility, which shows only a slight decrease. The only visible effect is on stiffness of cracking phase, that is lower for worst bond condition. In summary, we can conclude that the perfect bond condition is a reasonable hypothesis to be assumed, at least for the sound beams.

4.2.2 Corroded beams

The corroded beams (313 - 316) have been made with concrete type 2 and have been subjected to an accelerated corrosion process before being tested. Since the authors have not reported the actual distribution of corrosion penetration and the exact numbers of bars affected by pitting corrosion, some hypotheses are made in the numerical simulations: uniform corrosion is assumed for compressed bars and for two of the four tensed bars; instead mixed attack is considered for the other two tensed bars and for all the stirrups. This can be considered a suitable hypothesis because of the position of the bars: the two external tensed bars, located near the stirrup, are almost certainly subjected to the highest corrosion attack. The values of the corroded areas adopted in the numerical analysis are summarized in Table 5.

The constitutive law adopted for the concrete type 2, based on CEB-FIP MC 90 (1993) law, is amplified by the same *mesh size factor* used for concrete type 1. In order to take into account the deterioration of the concrete, due to the formation of micro and macro cracks in the cover, the approach described in Sect. 3.1 is adopted: the parameter d_{env} is introduced and the reduction of the compressive ductility of the concrete covers is evaluated according to equation (8).

As previously stated, to test and calibrate the main parameters necessary to define the degradation process, one of the corroded beam, i.e. the 313, is firstly simulated. Then all the other corroded beams are simulated by using the previously calibrated values of the parameters.

Table 5 Reduction of steel cross section due to corrosion attack – Beams type 31

Beam No.	Tensed bars			Compressed bars			Stirrups		
	Initial area [mm^2]	Residual area [mm^2]	Reduction [%]	Initial area [mm^2]	Residual area [mm^2]	Reduction [%]	Initial area [mm^2]	Residual area [mm^2]	Reduction [%]
313	452.39	383.98	-15.12	201.06	181.46	-9.75	28.27	8.04	-71.56
314	452.39	364.63	-19.40	201.06	175.77	-12.58	28.27	3.14	-88.89
316	452.39	359.06	-20.63	201.06	165.59	-17.64	28.27	2.27	-91.97
315	452.39	346.46	-23.42	201.06	168.33	-16.28	28.27	0.79	-97.21

Table 6 Reduction of compression strength of concrete cover due to corrosion – Beams type 31

Beam No.	Bottom concrete cover		Top concrete cover	
	Crack width [mm]	d_{env}	Crack width [mm]	d_{env}
313	1.88	0.69	1.26	0.60
314	3.02	0.78	1.63	0.66
316	2.64	0.76	2.32	0.74
315	3.20	0.79	2.14	0.72

Table 7 Reduction of compressive concrete cover ductility – Beams type 31

Beam No.	Reduction ductility concrete in bottom cover [%]	Reduction ductility concrete in top cover [%]
313	-30.24	-19.50
314	-38.80	-25.16
316	-41.26	-35.28
315	-46.83	-32.56

Table 6 summarizes the values of d_{env} for all the corroded beams, depending on crack width, while Table 7 lists the reduction of the ultimate strain of the deteriorated concrete obtained with (8).

Regarding the composite interaction between the concrete and the reinforcement, three different hypotheses are considered in order to carry out a sensitivity analysis: perfect adherence, good bond and degraded τ-s laws. Actually, for corroded beams, bond degradation phenomenon may affect the structural response of the elements. However, as previous stated for the tested beams, no influence of bond is pointed out by the experimental remarks, Rodriguez *et al*. (1996).

Other authors confirm such an observation: for example, Bertagnoli *et al*.(2006) state that, even if corrosion plays an important role on bond, the load carrying capacity of beams tested by Rodriguez are not much influenced by the bond reduction, up to a corrosion level of about 15% of the sectional area.

Calibration phase: beam 313

The beam 313 is the one subjected to accelerated corrosion for the shortest period. The depth of the corrosion attacks are reported in Table 3. As previously stated, two tensile bars are modeled with uniform corrosion and two with mixed corrosion, for all the length of the bars. Overall, a percentage reduction of 15% has affected the area of the tensile bars due to corrosion. Regarding the compressive bars, only a uniform penetration attack of 0.2 mm is observed. For this reason the reduction of the steel area is lower, about 10%. Finally, all the stirrups are considered affected by pitting corrosion as the worst condition, Table 5.

Concerning the reduction of ductility in compression of the cracked cover, for this beam different values of factor *f* are assumed, in order to calibrate the proposed formulation Eq. (8), leading to a choice for the *f* factor equal to 2, which is maintained for all the other corroded beams. Then, according to Eq. (8), the reduction of compressive concrete ductility for the bottom cover is resulted about 30%, while for the top one is around 20% (Table 7).

The constitutive laws adopted for the concrete core and the concrete covers are shown in Fig. 13. Fig. 14 depicts the Force-central displacement curve obtained by the numerical model,

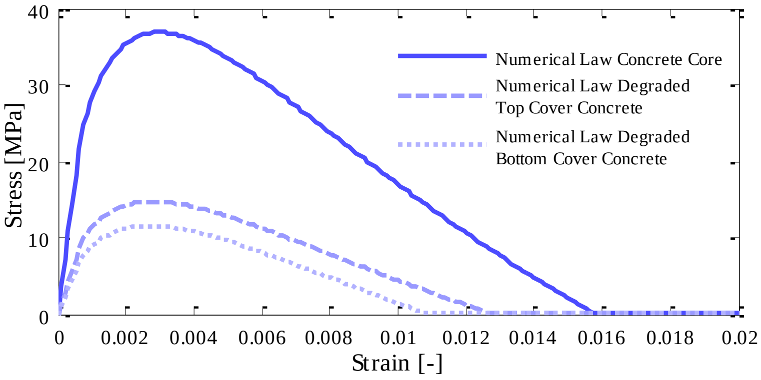

Fig. 13 Stress-strain curve for concrete core and concrete covers in corroded beam 313

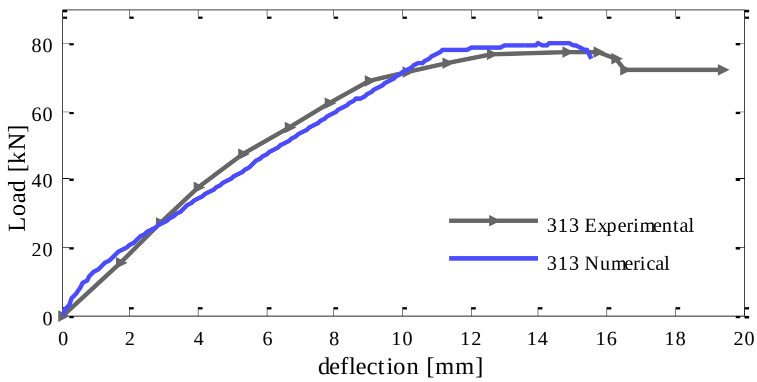

Fig. 14 Force-deflection curves for corroded beam 313

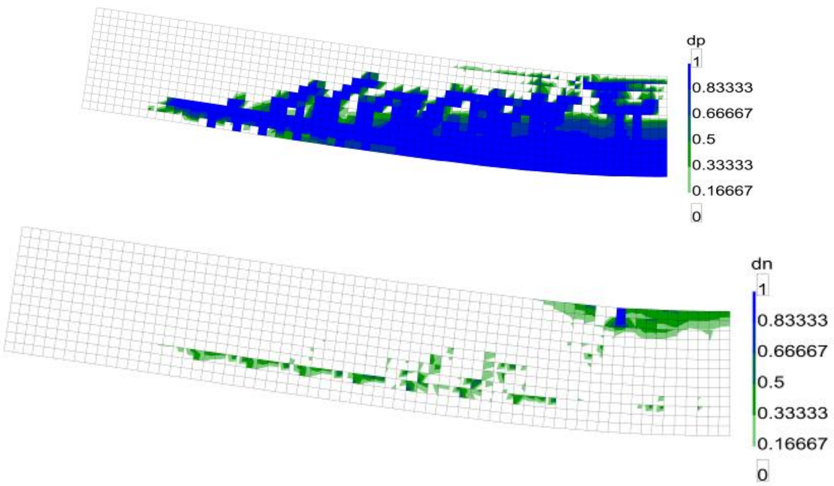

Fig. 15 Tensile (dp) and compressive (dn) damage contours for corroded beam 313

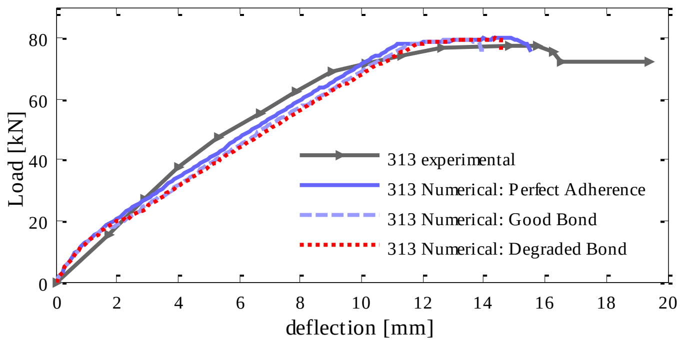

Fig. 16 Force-deflection curves for corroded beam 313 with different bond conditions

compared with the experimental one. The results confirm the good agreement obtained by the proposed approach in terms of both failure load and ultimate displacement, (the percentage error is respectvely less than 1 and 5%).

Finally, the damage contours at failure are reported in Fig. 15, confirming the crushing of concrete in compression, in the top concrete cover.

The numerical analyses are carried out with the condition of perfect adherence between the steel bars and the surrounding concrete. As for the sound beams, a sensitivity analysis about different bond condition is performed. In particular, two different bond stress-slip laws are conferred to the zero-length elements: the "Good Bond" condition provided by CEB-FIP MC 90 (1993) and the degraded τ–s law obtained applying the approach described in Sect 3.3. The numerical results obtained in the two hypotheses are shown in Fig. 16, in terms of force-displacement curves, compared with both the experimental and the perfect adherence results. Similarly to the case of sound beams, different bond stress-slip laws influence neither the failure load nor the ultimate displacement and only the stiffness of pre-yielding phase slightly changes, becoming lower for worst bond condition, as expected. Therefore, also for the corroded beams, the perfect adherence could be considered a reasonable approximation, since even the reduction of bond due to corrosion does not significantly influence the structural behaviour of such beams. Such results are in accordance with the experimental observations of non-influence of bond on structural response of such beams, e.g. Rodriguez *et al*. (1996), Castel *et al*. (2000), Bertagnoli *et al*. (2006).

Finally the sensitivity of the structural response to different evaluations of residual area of the tensile reinforcement is proposed. In detail, basing on the values of attack penetration reported in Table 3 for beam 313, five different methods to evaluate the residual area (Table 8), are examined and the corresponding diagram force-displacement are compared in Fig. 17.

By considering only pitting corrosion and the Val and Melchers (1997) proposal (i.e. case (c) of Table 8), the global response is very close to the one obtained without reduction of area (no corrosion case). Otherwise, by combining such a pitting area reduction with a uniform corrosion with $x = x_{mean} = 0.23$ mm (i.e. case (d) of Table 8), the obtained curve gets close to the experimental ones. Similar results are obtained by considering only uniform corrosion evaluated with $x=x_{mean}=0.30$mm, (i.e. case (a) of Table 8), confirming that the pitting corroded area evaluated with Val and Melchers (1997) proposal is very small for low pitting attacks, as demonstrated also by Fig. 5.

Table 8 Legend of Fig. 17 – Reduction of steel area: comparison between different approaches

(a)	Unifom corrosion Eq. (9) $x = x_{mean} = 0.30$ mm	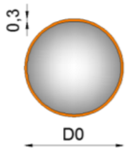	·4 bars
(b)	Mixed corrosion Eq. (10) p = 1.30 mm	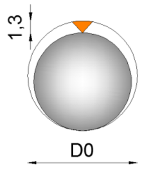	·4 bars
(c)	Pitting corrosion Val and Melchers, (1997) p = 1.30 mm	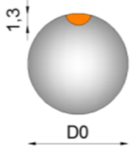	·4 bars
(d)	Pitting corrosion Val and Melchers. (1997) p = 1.30 mm and uniform corrosion x = 0.23 mm(*)	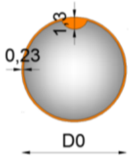	·4 bars
(e)	Mixed corrosion Eq. (10) p = 1.30 mm and uniform corrosion $x = x_{mean} = 0.30$ mm	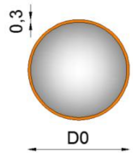	·2 bars
		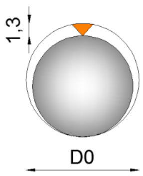	·2 bars

(*)value which takes into account an equivalence of gravimetric loss of steel area obtained in the experimental test.

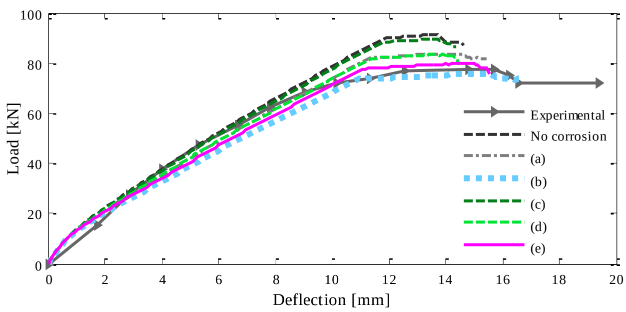

Fig. 17 Force-deflection curves for corroded beam 313 with different steel area reductions

The best results are obtained with case (b) and case (e) which refer respectively to the case of all the four bars subjected to mixed corrosion - Eq. (10)-, the second one (i.e. the hypothesis used in this paper) assumes the two external bars subjected to mixed corrosion – Eq. (10)- and the two internal bars subjected to uniform corrosion – Eq. (10) with $x=x_{mean}$=0.30 mm. Both these results are in good agreement with the experimental ones, confirming the suitability of Eq. (10) for evaluating residual area in case of mixed corrosion.

Predictive Phase: beams 314-315-316

Starting from the values of attack penetration and residual steel areas provided for such beams, summarized respectively in Table 3 and Table 5, and assuming the same numerical parameters obtained in the calibration phase, the responses of beams 314 to 316 are predicted.

The beams 314 and 316 are subjected to corrosion for a medium period, therefore they present halfway attack penetration between the beam 313 and the beam 315.

Concerning bond conditions, also for these beams a sensitivity analysis is carried out, Fig. 18. The results confirm that the degraded bond condition has not influence on the global response of such set of beams, as shown in the corresponding force-displacement graphs.

For both beams 314 and 316, the crushing failure of the compressive concrete cover occurred before that tensile bars had reached the yield stress. This experimental observation is correctly reproduced by the numerical simulation, as shown in the force-displacement graphs of Fig. 18

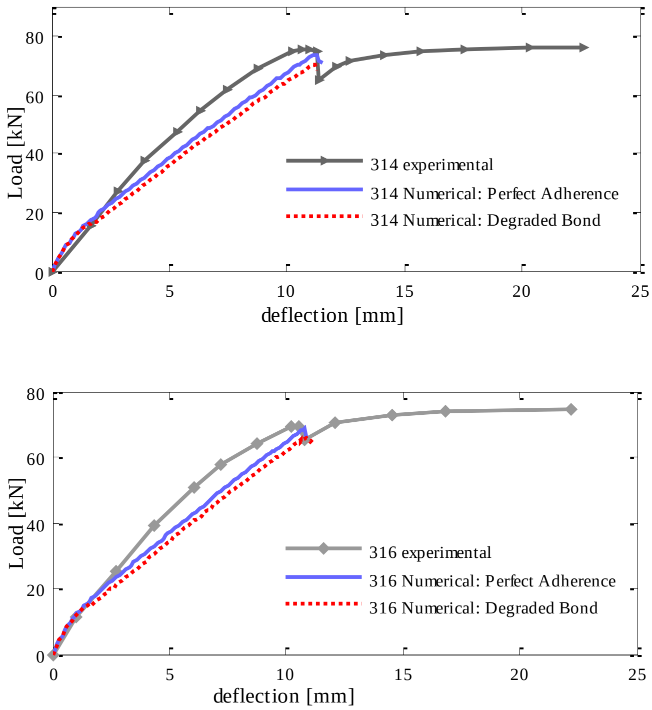

Fig. 18 Force-deflection curves for a) corroded beam 314 and b) corroded beam 316

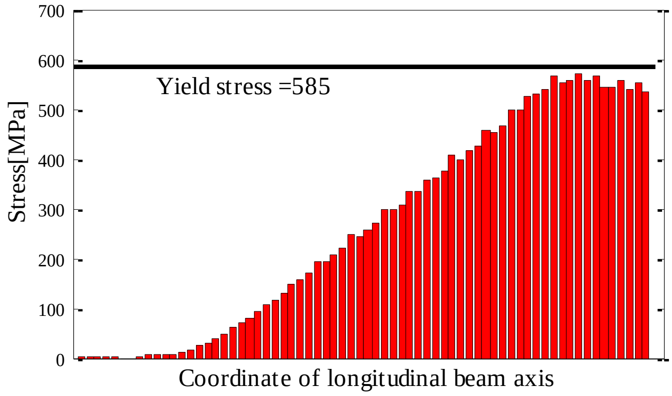

Fig. 19 Stress on the tensile bars of beam 316

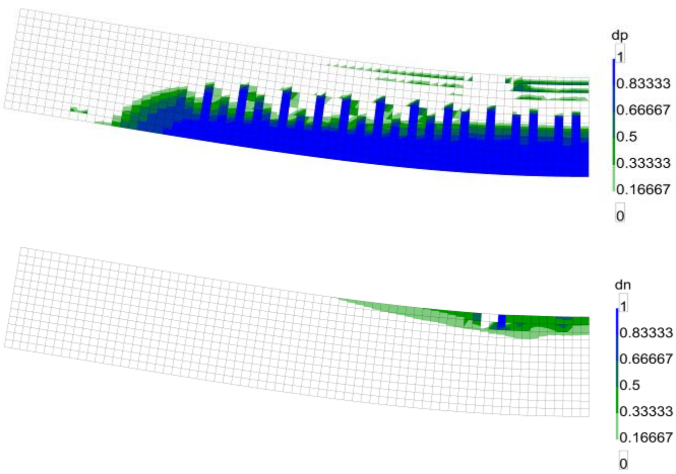

Fig. 20 Tensile (dp) and compressive (dn) damage contours for corroded beam 314

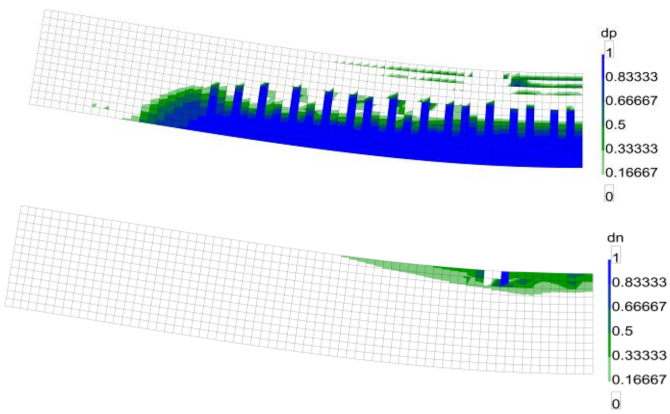

Fig. 21Tensile (dp) and compressive (dn) damage contours for corroded beam 316

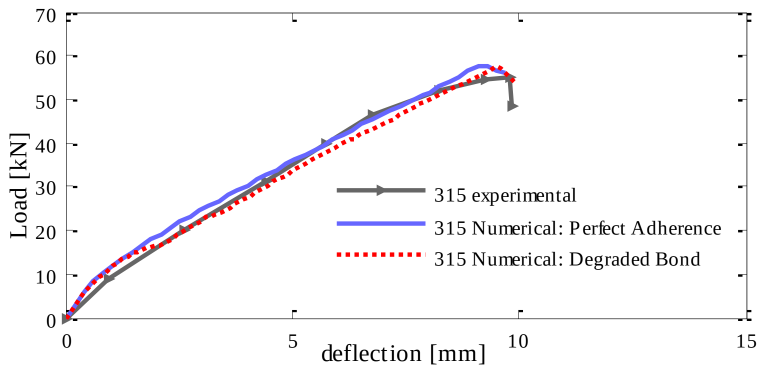

Fig. 22 Force-deflection curves for corroded beam 315

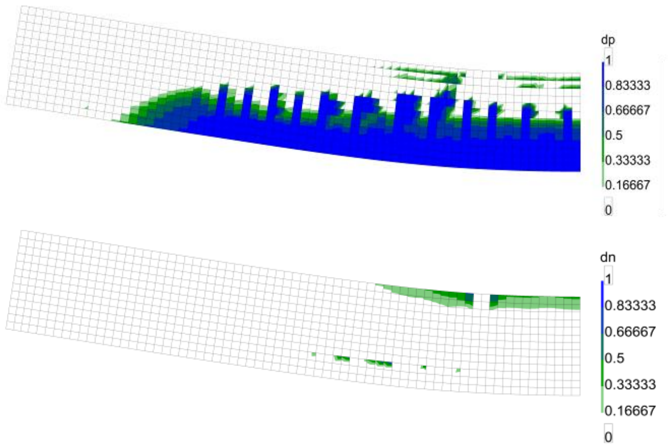

Fig. 23 Tensile (dp) and compressive (dn) damage contours for corroded beam 315

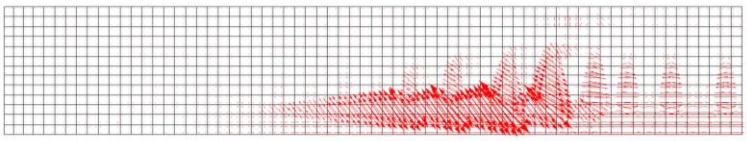

Fig. 24 Principal stress on corroded beam 315

for the beam 314 and 316, that demonstrate the absence of the ductile behaviour. It is worth noting that the slight increase of load in the experimental graph, after the load decrease, is ascribed by Rodriguez "to the collaboration of the sound part of the top concrete and the stress increase at tensile bars which had not reached the yield stress". Moreover, Fig. 19 shows the profile of stress along the longitudinal axis of the tensile bars for beam 316, always below the yielding value. Finally, Fig. 20 and Fig. 21 display the tensile and compressive damage contours for both the corroded beams, evidencing the failures by crushing in the compressed covers.

The beam 315 is the one subjected to corrosion for the longest period, therefore it presents the highest attack penetrations, especially for the stirrups. While the uniform and the pitting levels of corrosion for the tensile and the compressive bars are similar to beams 314 and 316, the stirrups present an attack penetration of pitting corrosion of 5 mm, starting from a diameter of 6 mm. This is probably the reason that provokes the change of failure mode: indeed, the beam 315 is the only one that exhibited a shear failure. Fig. 22 depicts the numerical and experimental force-displacement graph: it is worth noting that the model is able to well reproduce the high reduction of ductility and ultimate load, observed in the experimental test due to corrosion. The damage contour reported in Fig. 23 highlights the shear failure mode: actually, the tensile damage map shows the development of diagonal cracks at the failure step, while the compression damage map evidences that the damage in compression has not reached the maximum value of 1. Finally, as further confirmation of the shear mode of failure, Fig. 24 shows that the principal strains are disposed along the S-shaped path, typical of such a failure.

5. Conclusions

Reinforcement corrosion is the most important cause of deterioration in RC structures, because may lead to a high reduction of load carrying capacity and of ductility on the structural elements. Moreover, a change of type of failure, from the flexural to the shear one, can be observed in high degraded beams: this occurrence is particularly dangerous, especially in case of seismic events. For this reason, accurate methods to anticipate the response of deteriorated structures are necessary. In the present work a numerical approach, based on an environmental-mechanical damage model, enhanced to consider the corrosion effects in a comprehensive approach, is presented and validated against the experimental results of Rodriguez *et al*. (1996), Rodriguez *et al*. (1997). In the model, all the main local effects of corrosion phenomena are considered, in order to simulate the corroded beams behaviour. The good agreement between numerical results and experimental evidences, in terms of both force-displacement curves and mode of failure, demonstrates the capability of model to well capture the global structural response of corroded beams, for different levels of degradation.

In particular, the model is able to reproduce the failure mode both for the sound beams 311-312, i.e. with crushing in compression of the concrete long after that tensile bars had reached the yield stress, and for the corroded beams for which, with the increase of the level of corrosion, a reversal of the phenomenon is observed and the crushing of the concrete anticipated the yielding of the bars, (i.e. beams 314 and 316). Finally, for beam 315, the numerical model demonstrates its capability to reproduce also the effect of a level of corrosion so high to provoke a total loss of the structural ductility, with the anticipation of the shear cracking with respect to the flexural one.

In conclusion, concerning the set of experimental beams, the following conclusions may be made: the decrease of tensile reinforcement section and the effect of concrete cracking, are main issues for the evaluation of load carrying capacity reduction. The decrease of compressive ultimate strain of concrete is crucial for ultimate global ductility reduction, while the stirrups cross section reduction is particularly relevant for the change of failure mode of these beams (i.e. from bending to shearing).

Some more improvements to the proposed model may still be made in the future. In particular, two different environmental damage parameters in tension and in compression may be introduced: in this way different levels of degradations for compression and tension response can be considered. Within this context, it would be possible to develop a new damage environmental parameter for the compressive behavior of the concrete, able to take into account a different level of deterioration for the Young modulus, the ultimate strength and ultimate strain, linked to a certain level of reinforcement corrosion. The same approach could be adopted also for bond τ-s law.

Acknowledgements

Thanks are due to prof. Harald Budelmann for his profitable collaboration in the progress of the research and for valuable discussions.

References

Bertagnoli, G., Mancini, G. and Tondolo, F. (2006), "Bond deterioration due to corrosion and actual bearing capacity", In, *FIB 2nd International Congress*, Naples, Italy.

Berto, L., Saetta, A. and Talledo, D. (2014), "A coupled damage model for r.c. structures, proposal for a frost deterioration model and enhancement of mixed tension domain", *Constr. Build. Mater.*, **65** 310–320.

Berto, L. Simioni, P. and Saetta, A. (2008), "Numerical modelling of bond behaviour in RC structures affected by reinforcement corrosion", *Eng. Struct*, **30**, 1375-1385.

Bhargava, K., Ghosh, A.K. Mori, Y. and Ramanujama, S. (2007), Corrosion-induced bond strength degradation in reinforced concrete - Analytical and empirical models, *Nuc. Eng. Des.*,237,1140–57.

Biondini, F. and Vergani, M. (2012), "Damage modeling and nonlinear analysis of concrete bridges under corrosion. Roc. of 6th International Conference on Bridge Maintenance", *Saf. Manag.*, July 949-957.

Cabrera, J.G. (1996) Deterioration of concrete due to reinforcement steel corrosion. *Cement Concr Compos*,**18**,47-59.

Cairns, J., Plizzari, G.A., Du, Y., Law, D.W. and Franzoni, C. (2005), Mechanical properties of corrosion-damaged reinforcement. *ACI Mater J.*, **102**(4), 256-64.

Cape`, M. (1999), ''Residual service-life assessment of existing R/C structures'' MS thesis, Chalmers Univ. of Technology, Goteborg Sweden and Milan Univ. of Technology ~Italy, Erasmus Program.

Castel, A., François, R., Arliguie, G. (2000), Mechanical behaviour of corroded reinforced concrete beams-Part 2, Bond and notch effects, *Mater. Struct.*, **33**, 545-551.

CEB-FIP MC 90 (1993), Design of concrete structures. CEB-FIP Model Code 1990, CEB Bulletin d'Information 213/214, Thomas Telford, London.

Chung, L., Kim, J.J. and Yi, S. (2008) Bond strength prediction for reinforced concrete members with highly corroded reinforcing bars. *Cement Concrete Compos.*, **30**,603-11.

Coronelli, D. and Gambarova, P. (2004), "Structural assessment of corroded reinforced concrete beams modelling guidelines", *J Struct. Eng.*, **130**(8), 1214-24.

Du, Y.G., Clark, L.A. and Chan, A.H.C. (2005a), "Effect of corrosion on ductility of reinforcing bars", *Mag. Concrete Res.*, **57**(7), 407-490.

Du, Y.G., Clark, L.A. and Chan, A.H.C. (2005b), "Residual capacity of corroded reinforcing bars", *Mag. Concrete Res.*, **57**(3), 135-147.

DuraCrete. Modelling of degradation. (1998), *The European Union – Brite EuRam III. Project No. BE95-1347, Probabilistic Performance based Durability Design of Concrete Structures*, Report No. R4-5.

Faria, R., Oliver, J. and Cervera, M. (1998), "A strain-based plastic viscous-damage model for massive concrete structures", *Int. J. Solids Struct.*, **35**, 1533-58.

FIB MC 2010 (2013), Fib Model Code for Concrete Structures.Ernst & Sohn.

Finozzi, IBN, Berto, L., Saetta, A. and Budelman, H. (2014), "Numerical modeling of the corrosion effects on reinforced concrete beams", WCCM 2014, Barcelona 20-25 July 2014

Gonzalez, J.A., Andrade, C., Alonso, C. and Feliu, S. (1995), "Comparison of rates of general corrosion and maximum pitting penetration on concrete embedded steel reinforcement", *Cement Concrete Res.*, **25**(2), 257-264.

Hanjari, K.M., Kettil, P. and Lundgren, K. (2011), "Analysis of mechanical behavior of corroded reinforced concrete structures", *ACI Struct. J.*, **108**(5), 532-41.

Hanjari, K.M., Kettil, P. and Lundgren, K. (2013), Modelling the structural behaviour of frost-damaged reinforced concrete structures, *Structure and Infrastructure Engineering*, Maintenance, Management, Life-Cycle Design and Performance, **9**(5),416-31.

Kallias, A.N. and Rafiq, M.I. (2010), "Finite element investigation of the structural response of corroded RC beams", *Eng. Struct.*, **32**, 2984-2994.

Khan, I., François, R. and Castel, A. (2014), "Prediction of reinforcement corrosion using corrosion induced cracks width in corroded reinforced concrete beams", *Cement Concrete Res.*, **56**, February, 84-96.

Kobayashi, K. (2006), "The seismic behavior of RC members suffering from chloride-induced corrosion", *Proceeding of the 2nd Int. Congress, FIB.*

Lee, H.S., Noguchi, T. and Tomosawa, F. (2002), "Evaluation of the bond properties between concrete and reinforcement as a function of the degree of reinforcement corrosion", *Cement Concrete Res.*, **32**, 1313-1318.

Mckenna, F., Fenves, G.L., Scott, M.H. and Jeremic, B. (2000), "Open System for Earthquake Engineering Simulation (OpenSees)", Pacific Earthquake Engineering Research Center, University of California, Berkeley, CA.

Meng, L., Wang, T. and Wang F. (2011) "Experimental study on mechanical properties and impact on components for existing concrete of different service life". (in Chinese), *Proceeding of the International Conference of Electric Technology and Civil Engineering* (ICETCE).

Molina, F.J., Andrade, C. and Alonso, C. (1993), "Cover cracking as a function of bar corrosion, Part II - Numerical model", *Mater Struct*, **26**,532-548.

RILEM Report 14 (1996), In, Sarja, Vesikari, editors. Durability design of concrete structures. RILEM Report 14, London, E & FN Spon.

Rodriguez, J., Ortega, L.M., Casal, J. and Diez, J.M. (1996), Assessing structural conditions of concrete structures with corroded reinforcement. In, Dhir RK, Jones MR, editors. Concrete repair, rehabilitation and protection. E&FN Spon, p. 65-78.

Rodriguez, J, Ortega, L.M. and Casal, J. (1997), Load carrying capacity of concrete structures with corroded reinforcement. *Constr. Build. Mater.*, **11**(4), 239-48.

Rodriguez, J., Ortega, L. and Garcia, A. (1994), "Corrosion of reinforcing bars and service life of R/C structures, Corrosion and bond deterioration", *Proceeding of the International Conference on Concrete across Borders*, Vol. II, 315–326.

Saether, I. and Sand, B. (2009), FEM simulation of reinforced concrete beams attacked by corrosion, *ACI Structural J.*, **39** 3, 15-31.

Saetta, A. Scotta, R. and Vitaliani, R. (1998), "Mechanical behaviour of concrete under physical-chemical attacks", *J. Eng. Mech. ASCE*, **124**(10), 1100-1109.

Saetta, A., Scotta, R. and Vitaliani, R. (1999), "Coupled environmental-mechanical damage model of RC structures", *J. Eng. Mech.*,**125**(8), 930-940.

Scotta, R., Vitaliani, R., Saetta, A., Oñate, E. and Hanganu, A. (2001), "A scalar damage model with a shear retention factor for the analysis of reinforced concrete structures, theory and validation", *J. Comput. Struct.*, **79** (7),737-55.

Stanish, K., Hooton, R.D. and Pantazopoulou, S.J. (1999), "Corrosion effects on bond strength in Reinforced concrete", *ACI Struct. J.*, **96**(6), 915-922.

Val, D.V. and Melchers, R.E. (1997), "Reliability of deteriorating RC slab bridges", *J. Struct. Eng.*, **123**(12), 1638–1644.

Van Mier, J.G.M. (1984), Strain-softening of concrete under multiaxial loading conditions. PhD thesis, Eindhoven University of Technology, Eindhoven, The Netherlands.

Vergani, M. (2010), "Modellazione del degrado di strutture in calcestruzzo armato soggette a corrosione",

Degree Thesis, Politecnico di Milano, Italy (in Italian).
Vidal, T, Castel, A. and Francois, R. (2004), “Analyzing crack width to predict corrosion in reinforced concrete”, *Cement Concete Res.*, **34**,165-74.
Zhu, W.J. and François, R. (2013) Effect of corrosion pattern on the ductility of tensile reinforcement extracted from a 26-year-old corroded beam, *Adv. Concr. Constr.*, **1**(2), 121-136.

CC